ANALYSIS OF OBJECT OBSERVATIONS
USING A 1.8-METER TELESCOPE

Paul Kervin[1], Paul Sydney[2], Mark Bolden[1], Tom Kelecy[3]

[1]*Air Force Research Laboratory, 535 Lipoa Parkway, Suite 200, Kihei HI 96753, USA*
[2]*Pacific Defense Solutions, 590 Lipoa Parkway, Suite 217, Kihei HI 96753, USA*
[3]*Boeing LTS, Inc., 5555 Tech Center Drive, Colorado Springs, CO 80919, USA*

ABSTRACT

The Pan-STARRS (Panoramic Survey Telescope & Rapid Response System) is a telescope system designed by the University of Hawaii Institute for Astronomy. The prototype telescope system is located on Haleakala, on Maui, Hawaii. This prototype has a 1.8 meter aperture with a field of view of more than 7 square degrees. The 1.4 gigapixel camera is a novel design based on Orthogonal Transfer Arrays (OTA). Although designed for an astronomical mission, this telescope can be used to search for faint objects in near-geosynchronous orbit by turning off sidereal track during the exposure. This paper discusses unique aspects of the design of the telescope that make it very powerful for geo search, the search strategy used, and the results of the survey of the geo belt.

1. INTRODUCTION

The Panoramic Survey Telescope and Rapid Response System (PAN-STARRS) is a telescope designed and built by the University of Hawaii Institute for Astronomy for an astronomical mission. The telescope has been described in other publications [3,4,5], so only basic information will be provided in this paper. The prototype telescope system (PS1) is located at the 3-km summit of Haleakala on the island of Maui, in Hawaii. The aperture of the telescope is 1.8 meters, and provides a field of view of more than 7 square degrees. The camera is a 1.4 gigapixel (38k by 38k) device, consisting of 60 orthogonal transfer arrays (OTAs), each of which is an 8x8 array of orthogonal transfer charge coupled devices (CCDs). The plate scale is approximately 0.26 arcseconds per pixel, resulting in highly accurate position information. The size of the data file associated with each exposure frame is 2.8 gigabytes, generating several terabytes of data on a typical night of observations.

Although the system was designed for astronomical purposes, with a sidereal tracking mode, it can be used for observing Earth-orbiting satellites by turning the tracking mode off, staring at a fixed azimuth and elevation. This effectively optimizes the observations for satellites in geostationary orbit. The stars streak through the field of view in this scenario, while the light reflected from a geostationary satellite is concentrated in just a few pixels. The sensitivity for satellites in other orbits decreases, since the light reflected from those satellites appear as streaks, spreading the light over a larger number of pixels.

The prototype system will be operational for routine use in the Spring of 2009. During the telescope commissioning phase, several nights have been made available to use this telescope for observations of Earth-orbiting satellites, in August of 2008, and in December of 2008.

2. SEARCH STRATEGY

We used the telescope to search for objects visible over Maui during the two nights of observations in 2008. The strategy that we used is based on the strategy often used by the Inter-Agency Debris Coordination Committee (IADC) described in the reference by Africano and Schildknecht [1,2]. The telescope is pointed at a number of fields adjacent in declination (dec), but constant in right ascension (ra). This means that the star fields observed are the same throughout the night. This enables optimized techniques to detect and process the star images. At each of these ra and dec fields, the telescope drive is turned off, resulting in a field where the stars streak from east to west, and any geostationary satellite appears to be motionless. This technique has greatest sensitivity to geostationary objects, with lesser sensitivity associated with all other orbits.

Fig. 1 shows an implementation of this strategy, where the three rectangles represent the slightly overlapping fields of view, which remain fixed to the star background. Although the fields themselves always begin at the same ra and dec, the telescope is fixed during the exposure, so that the image is similar to what is shown in Fig. 2. This figure shows a single OTA. Note that all of the stars are streaking through the field of view, but there is an apparently geostationary object, shown within the circle.
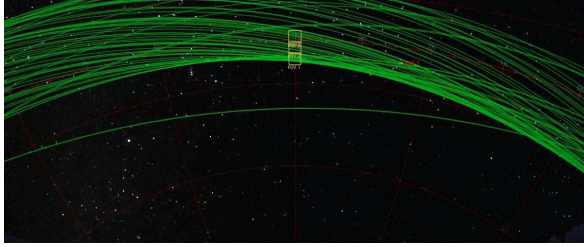
Fig. 1. View of GEO Belt Search in Declination at a Fixed Right Ascension
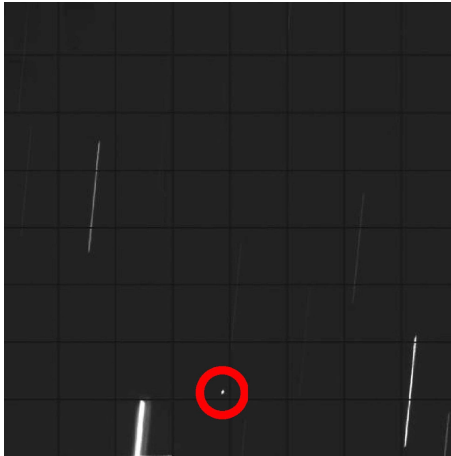

Fig. 2. Example Image with GEO Object and Star Streaks

The trade-offs for this type of search strategy include the selection of the right ascension, the number of declination fields, the overlap between declination fields, the integration time, and the selection of the optical filter used during observations. This search can be optimized for purely geostationary objects, in which case there would be a single declination field. This would truly be a leak-proof fence (in the absence of weather outages). However, as the orbits of objects deviate from geostationary, the objects may pass above or below that declination field. It is for this reason that we may use several declination fields, to capture objects with non-zero inclinations or eccentricities.

3. DATA REDUCTION

The data reduction and analysis algorithms used on Pan-STARRS have been developed over several years for other sensors. However, there are specific challenges in employing these techniques on the PS1 system. An overview of the algorithms is shown in Fig. 3, where PS1 specific enhancements are blocks highlighted with thick outlines.
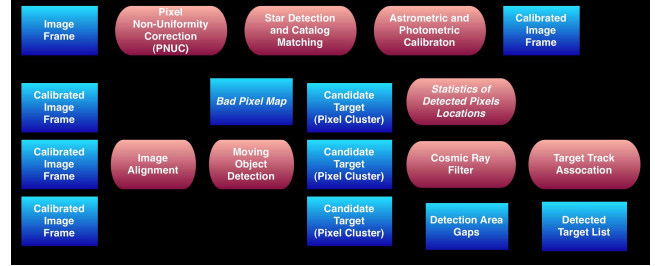

Fig. 3. Pan-STARRS (PS1) Data Reduction and Analysis Process

The PS1 sensor is a mosaic of 60 separate chips, which in aggregate, results in an enormous number of pixels to process. The algorithms are configured as processing stages where each of 60 chips can be executed separately until the last processing stage, "Target Track Association". This allows the algorithms to process in near real-time on a cluster of computer nodes. The number of pixels also poses a challenge in terms of false alarm statistics. The algorithm used in the "Moving Object Detection" stage is based on combining a stack of N image frames in Constant False Alarm Rate (CFAR) Detection with threshold, T defined as:

$$P_{max} - P_{avg}(w/o\ max) > T \cdot \sigma_P(w/o\ max) \qquad (1)$$

where P_{max} is the maximum pixel value in the image stack and P_{avg} and σ_P are the mean and standard deviation of the remaining pixels in the stack excluding P_{max}. In current processing, the pixels are 3x3 binned so the pixel Instantaneous Field of View (IFOV) is near the nominal imaging spot size. Even with the 9X reduction in total pixels, the CFAR algorithm with a detection threshold of 4.3σ will still produce 2600 false alarms per image frame as shown in Fig. 4.
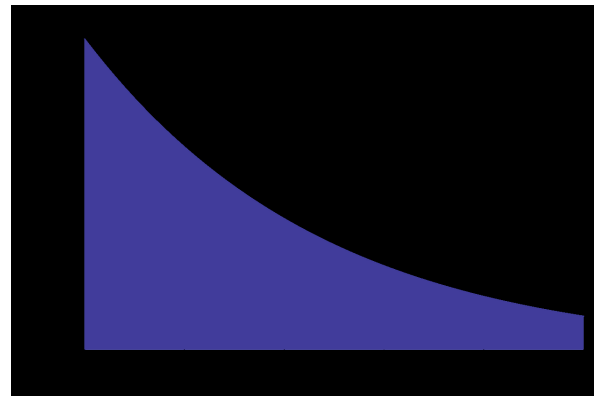

Fig. 4. False alarm statistics based on detection threshold

Since these false alarms are based on single pixel statistics, by requiring 2 or more adjacent pixels for a

valid detection, the number of false alarms is greatly reduced. This adjacent pixel requirement also reduces detection sensitivity, but it is not significant since the imaging spot size is greater than the pixel IFOV.

A second challenge to processing is that the current PS1 Pixel Non-Uniformity Correction (PNUC) does not address pixel response non-linearity, i.e. "warm pixels" which can create false targets. Our approach, as depicted in Fig. 3, is to perform the "Moving Object Detection" stage twice. In the first pass, the pixel location of detections is compared over many observations and pixels producing frequent detections are added to a bad pixel map. All valid targets in the PS1 images are moving over time, so only poorly responding pixels will be detected frequently. The second "Moving Object Detection" pass ignores these high detection rate pixels and produces the final list of detection candidates. For PS1, <0.1% of the pixels have been masked by this filter. In the future, a dome-mounted calibration screen containing "leaky optical fibers" fed by a monochromator will determine pixel response linearity and reduce the number of potential false alarms [9].

Another challenge is that the 0.143 m^2 PS1 array with 75μm CCD thickness results in 200-300 cosmic ray hits per exposure with an average length of 3-4 pixels in 3x3 binning [8]. The final "Track Association" stage shown in Fig. 3 does help reduce the number of false alarms produced by cosmic rays, but cosmic rays compared over 8 to 10 frames can produce track candidates. Cosmic ray filtering based on simple shape parameters or PSF fitting has had limited success. Our new approach is to implement the Laplacian Edge Detection Algorithm for detecting cosmic rays [10]. The algorithm can be computationally intensive, but by applying the algorithm to pixel clusters produced by the "Moving Object Detection" step, the processing requirements can be greatly reduced.

A final challenge is due to the detection area gaps in the sensor. A combination of hot, bad, and warm pixels along with the physical separation between CCDs results in 7-11% loss in the total sensor detection area. The M out of N detection scheme used in the "Target Track Association" stage allows for some missing detections. However, there are some cases dependent upon the observation cadence where a target is not visible in M frames. To address this issue, when detections are paired to form the endpoints of a potential track; intermediate detection points are counted if they fall in a detection loss area. As a rule of thumb for PS1 with a 9-image stack, 3 detections predicted in loss areas are considered a single valid detection and added to the M out of N detection criteria.

Observations collected in December 2008 have allowed an estimate of PS1 detection sensitivity in GEO search mode. The detection sensitivity is based on the following parameters:

- 3x3 pixel binning
- Observed in Sloan Digital Sky Survey (SDSS) "w" filter
- 5-second exposure time
- Airmass ranged 1.15 to 2 (zenith angle of 30° to 60°)
- Binned IFOV: 3.7 μrads (0.75 arcsecs)
- Spot size (FWHM): 4.1 μrads (0.85 arcsecs)
- Sensor gain: ~1 e- / DN
- Sensor noise: < 8 e-
- Sky background: 350 – 550 e- (20.5 – 21 Mv / arcsec^2)
- Total measured RMS noise (σ): 20 – 24 e- (varies with airmass)
- Detection threshold: 4.3σ
- Minimum detection size: 3 pixels

Using these value for an airmass of 1.15, the nominal detection sensitivity is ~21.5 magnitudes in the SDSS "w" filter. The faintest target detected on 2 Dec was 21.0 magnitudes.

4. DATA ANALYSIS

Using the search method described earlier, we can observe a geostationary object many times as it passes through this star field, the number depending on the parameters listed above. No matter how many times we detect the object, we see the object over approximately a 10-minute portion of its orbit. For a geostationary object, this is less than 1% of its orbit. That makes it very difficult to obtain a good orbit from the data, even with low noise and accurate position information.

For our analysis we used Gauss' method to determine an initial guess at the orbit using 3 of the ra/dec observation pairs for an object. We then used that initial guess as an input to a fit minimizing the least-squares error, using all of the observations to refine the orbit estimate. A large *a priori* covariance is assumed to account for the large initial uncertainty. This yields a description of the 6-parameter orbit in terms of the classical orbital elements. Since the observations only provide data over a relatively short segment of the true orbit, the quality of the mean motion and eccentricity (n and e) in these solutions is in question. However, the orbit orientation parameters, inclination and right ascension of ascending node (i and Ω) should be fairly adequately determined with the available data.

We obtain the visual magnitude of the observed object using the star background as our fiducial. This magnitude, combined with the inclination of the orbit and the right ascension of ascending node (RAAN), from our rough orbit determination, provide a fingerprint of each satellite. This fingerprint will remain valid for weeks or even months, for most GEO satellites, within the uncertainty of the estimated parameters. There will certainly be cases for which this is not true. For example, small objects with high area to mass ratios will experience more dramatic effects due to non-conservative forces. Nevertheless, these quantities can be useful in comparing satellite observations over short periods of time.

For example, in Fig. 5, we plot inclination versus magnitude of the objects from Aug 2008 for which we could obtain a solution. For a fingerprint to be useful, the values should be widely dispersed in the fingerprint parameter space. This is the case for the satellites plotted, with the exception of a clustering of rather bright satellites with low inclination. These satellites are most likely active, cataloged objects, for which accurate element sets are available and are less needful of fingerprinting.
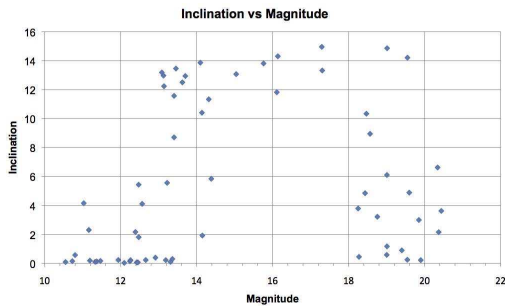

Fig. 5. Inc vs. Mag for August 2008 Observations

However, this plot leaves out one of the fingerprint parameters, RAAN. If we plot RAAN vs. inclination, and let the size of the bubble indicate the satellite brightness, we can display all three parameters on the same plot. This is what is shown in Fig. 6 for the August 2008 data. Note the additional dispersion throughout the RAAN - Inclination parameter space. Of course, RAAN is undefined for inclinations of zero degrees, and poorly determined for inclinations close to zero degrees in this initial orbit determination, so one should treat the RAAN values for inclinations near zero with some skepticism. In Fig. 7 we show the same plot for the observations from December 2008. Note that in the December data we find no inclinations greater than 12 degrees, in contrast to the August 2008 data. In Fig. 8 we plot both data sets on the same plot.
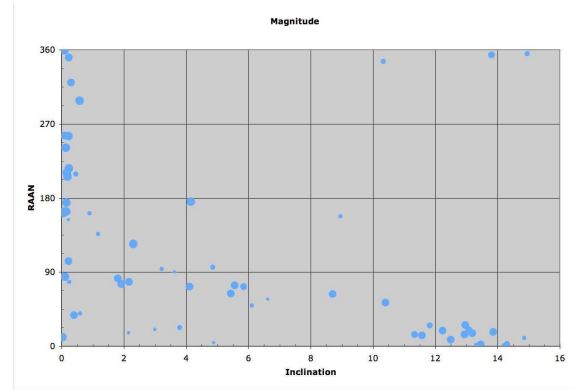

Fig. 6. August 2008 Observation Magnitudes Plotted as RAAN vs. Inclination
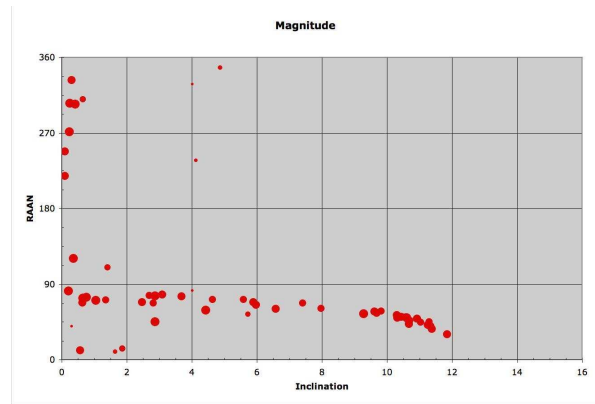

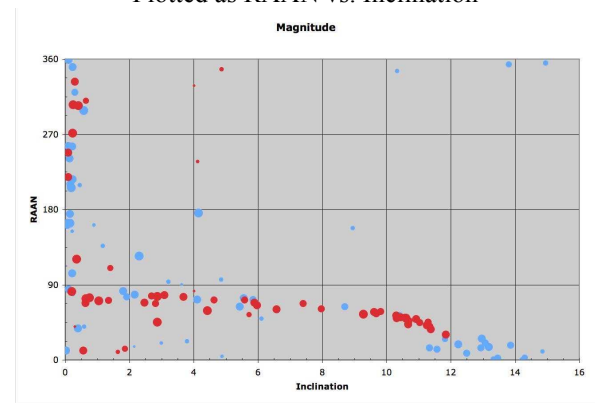Fig. 7. December 2008 Observation Magnitudes Plotted as RAAN vs. Inclination

Fig. 8. Combined Observation Magnitudes Plotted as RAAN vs. Inclination

There are notable differences in the parameter distributions between the August 2008 and December 2008 data. There are a number of likely causes for this. The December data was much cleaner than the August data due to improvements in the telescope optics and data processing. It is expected that the noise levels for

subsequent observation runs will be improved further over the December 2008 data.

An even broader question is why the satellite parameters themselves appear to represent different satellite populations. Remember that there is a four-month difference in the observation times. For one thing, it is possible that the values of the parameters have changed over that time period. It is not uncommon for object inclinations and RAANs to change by several degrees over this time period. In addition, there is an uncertainty in the values of these parameters derived from the observations. Of course, it is also likely that we are not looking at the same satellite population. Although the bright objects with low inclinations are most likely the same, the other objects could be different populations due to the satellites drifting slowly past the observation site, or it could be to objects that were missed by the admittedly leaky observation "fence." Future work will examine correlation between tracks collected at different times over the same region of sky.

Fundamentally, the parameters we've chosen for fingerprinting should be quite stable over relatively short periods of time. During the next set of observations, which should include observations on back-to-back nights, the satellite populations should be very similar, so many of these sources of differences will be eliminated. Furthermore, the correlation of tracks taken over several nights will allow for more accurate orbit determination, thus reducing a major remaining source of error. There is a very good chance that we can use these fingerprints to suggest likely night-to-night associations to help with the track correlations. This should be aided by the wide spread of satellite positions in this parameter space.

5. CONCLUDING REMARKS

Care should be taken in interpreting the data from these two runs in any statistical fashion due to the limited numbers. We don't yet have the luxury of years of observing the satellite environment that other programs have [7]. However, it appears that there is great potential for using PS1 to contribute to future observing campaigns, and to help to characterize the orbits of resident space objects in the GEO orbit regime.

Sensitivity of the system should increase over the next year as the data generated by the PS1 system becomes much more consistent, and the data reduction and processing techniques are improved. This is particularly true as we develop more techniques and algorithms to take advantage of the unique capabilities of the orthogonal transfer devices.

Fingerprinting the satellites in the parameter space defined by the visual magnitude, the inclination, and the RAAN looks very promising. Adding in the variability of the visual magnitude over multiple observations of a satellite on each night should also increase the parameter space, and more uniquely characterize the satellite, yielding a powerful tool to assist in linking night-to-night observations.

6. REFERENCES

1. Africano, J., Schildknecht, T., "International Geostationary Observational Campaign," *IADC AI12.1 Report*, September 2000.

2. Africano, J., Schildknecht, T., Matney, M., Kervin, P., Stansbery, E., Flury, W., "A Geosynchronous Orbit (GEO) Search Strategy," *Space Debris*, v. 2 n. 4, 357-369, 2004.

3. Kaiser, N. et al, "Pan-STARRS – A New Generation Survey Telescope System," *Proceedings of the 2006 AMOS Conference*, 376-385, 2006.

4. Kervin, P., "A survey of wide-field-of-view optical telescopes," *7th US/Russian Space Surveillance Workshop Proceedings*, 145-152, 2007

5. Kervin, P., Sydney, P., Bolden, M., Jah, M., Use of an Astronomical Telescope to Search for Earth-Orbiting Objects, *59th International Astronautical Congress Proceedings*, 29 Sep – 3 Oct 2008.

6. Morgan, J., Siegmund, W., Hude, C. et al, "The design of the Pan-STARRS telescope #1," *Proceedings of the 2006 AMOS Conference*, 402-411, 2006.

7. Schildknecht, T., Musci, R., Flohrer, T., "Challenges Related to Discovery, Follow-up, and Study of Small High Area-to-Mass Ratio Objects at GEO," *Proceedings of the 2007 AMOS Conference*, 354-358, 2007.

8. Smith, A.R. et.al., "Radiation events in astronomical CCD images," *IS&T/SPIE's Electronic Imaging*, 23 Jan 2002.

9. Tonry, J.; Stubbs, C.; Masiero, J.; "The Pan-STARRS PS1 Calibration System", *Proceedings of the 2006 AMOS Conference,* 441, 2006.

10. van Dokkum, Peter G.; "Cosmic Ray Rejection by Laplacian Edge Detection", *Publications of the Astronomical Society of the Pacific*, 113, 1420-1427 2001.